CURRENT STATUS OF THERMAL/HYDRAULIC FEASIBILITY PROJECT FOR REDUCED- MODERATION WATER REACTOR (2) - DEVELOPMENT OF TWO-PHASE FLOW SIMULATION CODE WITH ADVANCED INTERFACE TRACKING METHOD

HIROYUKI YOSHIDA*, HIDESADA TAMAI, AKIRA OHNUKI, KAZUYUKI TAKASE and HAJIME AKIMOTO
Japan Atomic Energy Agency
2-4, Shirakata Shirane, Tokai, Ibaraki, Japan
*Corresponding author. E-mail : yoshida.hiroyuki@jaea.go.jp

Received February 3, 2006

We start to develop a predictable technology for thermal-hydraulic performance of the RMWR core using an advanced numerical simulation technology. As a part of this technology development, we are developing the advanced interface tracking method to improve the conservation of volume of fluid. The present paper describes a part of the development of the two-phase flow simulation code TPFIT with the advanced interface tracking method. The numerical results applied to large-scale water-vapor two-phase flow in tight lattice rod bundles are shown and compared with experimental results. In the results of numerical simulation, a tendency of the predicted void fraction distribution in horizontal plane agreed with the measured values obtained by the advanced neutron radiography technique including the bridge formation of the liquid at the position of adjacent fuel rods where an interval is the narrowest.

KEYWORDS : Numerical Simulation, RMWR, Two-phase Flow, Advanced Interface Tracking Method, TPFIT

1. INTRODUCTION

As a nuclear reactor for the future, the fast breeder reactors using liquid metal sodium as the coolant (LMFBRs) are under development, and or supposed to take the place of the light water reactors (LWRs) in the future nuclear power generation. The development, however, is delayed a lot, and hence, it is prospected for the light water reactors to continue to be utilized for some time and to play an important role as the nuclear reactors in the future. Based on this situation, concepts of advanced water-cooled reactors suitable for the future have been investigated at the Japan Atomic Energy Research Institute (JAERI) [1, 2]. They are named reduced-moderation water reactor (RMWR) with the high conversion ratio around 1.0 by using Pu-MOX fuel as the seed fuel.

In the RMWR core, remarkably narrow gap spacing between rods (about 1 mm) is used to reduce the moderation of the neutron. To optimize the thermal design, boiling transition (BT) in such a tight lattice core is one of the most important subjects to be evaluated, but effects of the gap and spacer configuration have not been fully investigated. To evaluate the feasibility and to optimize the thermal design, a full-scale bundle test is required but several systematic full-scale tests are difficult to be performed during an initial design phase.

Thus, we start to develop a predictable technology for thermal-hydraulic performance of the RMWR core using an advanced numerical simulation technology. As a part of this technology development, we are developing an advanced interface tracking method to improve the conservation of volume of fluid.

The present paper describes a part of the development of the two-phase flow simulation code TPFIT with the advanced interface tracking method. The vectorization and parallelization of TPFIT code was conducted to fit the large-scale simulations. In this paper, detail of advanced interface tracking method is described, and numerical results performed to verify applicability of TPFIT for two-phase flow are shown. Furthermore, the numerical results applied to large-scale water-vapor two-phase flow in tight lattice rod bundles are shown and compared with experimental results.

2. NUMERICAL PROCEDURES

2.1 Advanced Interface Tracking Method

To get detailed information about two-phase flow in the nuclear reactor core, compressibility of fluid must be evaluated. Then, we developed an advanced interface tracking method can treat compressible flow including gas-liquid interface. The vectorization and parallelization of the simulation code were considered in development of the interface tracking method. And the Cartesian coordinates and the staggered grid were adopted in the method. The outline of advanced interface tracking method is divided into four parts shown as below.

1) Decomposition of interface to segments
2) Lagrangian propagation of interface segments
3) Reconfiguration of interface
4) Calculation transport equations of density

Firstly, the advanced interface tracking method approximates the gas-liquid interface with a linear function: F(***x***) as same as PLIC method [3]. Function F(***x***) is expressed as follows:

$$F(\mathbf{x}) = \sum_{i=1}^{n_m} a_i x_i + b \,. \tag{1}$$

In the equation, n_m represents dimension of simulation, and equals 2 or 3. x_i is the coordinate position of the definition point of scalar quantities. A unit normal vector to the interface **a**= (a_1,a_2,a_3) and segment b in eq. (1) must be estimated.

To approximate the interface by linear function, we assumed that the interface exists in the position where volumetric fraction: f_m equals 0.5. By least-squares method (choose eight nearest neighbors for 2-dimensional case), linear function is obtained.

$$F(\mathbf{x}) = f_m - 0.5 = \sum_{i=1}^{n_m} a_i x_i + b_0 \,. \tag{2}$$

In the equation, b_0 is preliminary segment.

Interfaces are divided into small segments by using the linear functions. In Fig. 1, "V_m" is the volume of the polygon that is made by the linear plane and calculation grid boundary. The volume of the polygon, V_m, must equals proper volume of each fluid. Thus,

$$V_m = f_m \Delta V \tag{3}$$

where ΔV is a volume of computational cell given by following equation for 3-dimensional cases.

$$\Delta V = \Delta x_1 \cdot \Delta x_2 \cdot \Delta x_3 \tag{4}$$

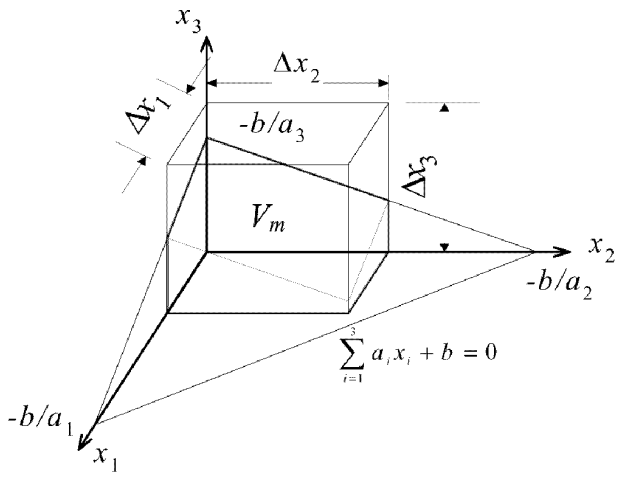

Fig. 1. Approximated Fluid Segment in Numerical Cell (3-dimensioncal case)

To satisfy eq. (4), the segment "b" is adjusted as fraction $V_m/(\Delta x_1 \cdot \Delta x_2 \cdot \Delta x_3)$ agrees with volumetric fraction of fluid. Between the volume of fluid V_m and segment b, there is the relation that is expressed as the following equation for two dimensional cases.

$$V_m = \frac{1}{2a_1a_2}\left\{b^2 - \sum_{i=1}^{2}\left[\max\left(b - a_i\Delta x_i, 0\right)\right]^2\right\} \tag{5}$$

For three dimensional cases, following equation is applied.

$$V_m = \frac{1}{6a_1a_2a_3}\left\{b^3 - \sum_{i=1}^{3}\left[\max\left(b - a_i\Delta x_i, 0\right)\right]^3 - \sum_{i=1}^{3}\left[\max\left(b - b_m + a_i\Delta x_i, 0\right)\right]^3\right\} \tag{6}$$

In the equation, b_m is the maximum value that "b" can take:

$$b_m = \sum_{i=1}^{3} a_i \Delta x_i \,. \tag{7}$$

In this study, the Newton's method is used to estimate the segment "b" that satisfies eq. (6) or (7). Using linear function and computational cell boundaries, the gas-liquid interfaces can be divided to small segments.

These small segments move in accordance with flow field. Figure 2 shows computational cells arrangement considering movement of gas-liquid interface. The small segment is located in the cell (i, j), and nine cells (eight

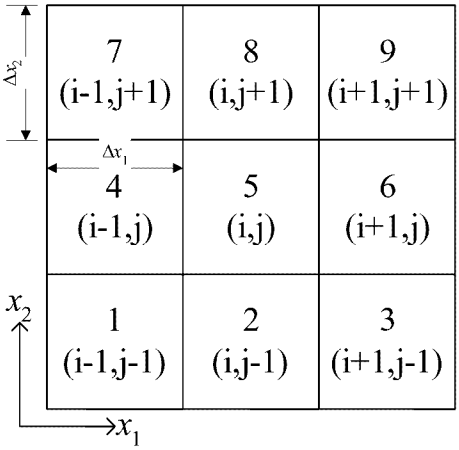

Fig. 2. Computational Cell Arrangements

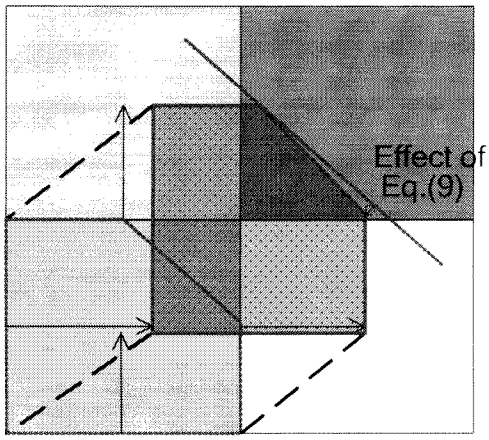

Fig. 3. Convection and Distortion of Fluid Segment

nearest neighbors for 2-dimensional case and center) are numbered from 1 to 9 shown as Fig. 2. The area of polygon ($V_{m,i,j}$) is distributed to surrounding computational grid (see Fig. 3). To estimate the movement of the small segment, the change of linear function and movement of computational cell boundaries in terms of flow field must be evaluated. As shown in Fig. 3, the linear function calculated by the least square method to approximate the interface is changed in accordance with flow field:

$$F'(\mathbf{x}) = \sum_{i=1}^{n_m} a'_i x_i + b' \tag{8}$$

$$a_i' = a_i + \left(\sum_{k=1}^{n_m} a_k \frac{\partial u_k}{\partial x_i} \right) \Delta t \tag{9}$$

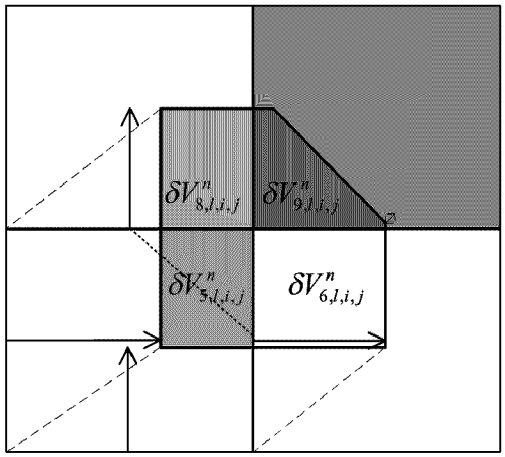

Fig. 4. Transfer Rate of Volume Between Numerical Cells in the Case of Two-dimensional Simulations

$$b' = b + \left(\sum_{i=1}^{n_m} a_i \cdot u_i \right) \Delta t \tag{10}$$

where Δt is time interval of simulation and u_i is velocity component of the small segment. In the eq. (9), the second term represents the effects of rotation and deformation of the segments. Equation (10) shows the effect of the parallel movement in terms of flow fields.

In Fig. 4, the overlapping area of the segment and the numerical cell becomes volume transfer rate for each numerical cell. In this paper, these volume transfer rates are defined with $\delta V_{m,i,j}$.

Using the volume transfer rate between the numerical cells, the volumetric fraction at new time step is evaluated by the following equation:

$$f^{n+1}_{m,i,j} = \frac{\sum_{l=1}^{9} \delta V_{m,l,i+li,j+lj}}{\Delta V_{i,j}} \tag{11}$$

where n+1 indicates new time step value. li and lj are indexes of the surrounding cells, and given by following equations:

$$\begin{aligned} li &= 1 - \mathrm{mod}(l-1,3) \\ lj &= 1 - \mathrm{mod}\left[\mathrm{int}\left(\frac{l-1}{3} \right) - 1,3 \right] \end{aligned} \tag{12}$$

In this interface tracking method, Navier-Stokes equations for compressible flow are used as basic equations. Therefore, the volume is not conserved fundamentally, and preserved indirectly through the conservation of mass. So, the mass transport needs to calculate with the accuracy similar to the volumetric fraction. To obtain the solution

of sufficient accuracy without doing the iteration to solve the pressure and density calculation that are required in the compressible fluid simulation, we would solve the mass transport equations by the same procedure for the volumetric fraction. Then, the density in new time step is evaluated by the following equation:

$$\rho_{m,i,j}^{n+1} f_{m,i,j}^{n+1} = \frac{\sum_{l=1}^{9} \rho_{m,i+li,j+lj}^{n} \delta V_{m,l,i+li,j+lj}}{\Delta V_{i,j}} \tag{13}$$

Because the volumetric fraction in the new time step is evaluated in eq. (11), the density in new time step is given as follows.

$$\rho_{m,i,j}^{n+1} = \frac{\sum_{l=1}^{9} \rho_{m,i+li,j+lj}^{n} \delta V_{m,l,i+li,j+lj}}{\sum_{l=1}^{9} \delta V_{m,l,i+li,j+lj}} \tag{14}$$

2.2 Basic Equations

Developed interface tracking method was incorporated to the detailed two-phase flow simulation code: TPFIT [4]. In the TPFIT code, considering the time-dependent Navier-Stokes equation for compressible flow, the conservative equations of mass, momentum and energy are described as follows;

Mass:

$$\frac{D\rho}{Dt} = -\rho \frac{\partial u_i}{\partial x_i} \tag{15}$$

where, density ρ is calculated using the densities and the volumetric fractions of both phases.

$$\rho = \rho_l f_l + \rho_g f_g, \quad f_g = 1 - f_l \tag{16}$$

Momentum:

$$\frac{Du_i}{Dt} = -\frac{1}{\rho}\frac{\partial p}{\partial x_i} + \frac{1}{\rho}\frac{\partial \tau_{ij}}{\partial x_j} + g_i + \sigma_i \tag{17}$$

Energy:

$$\frac{De}{Dt} = -\frac{p}{\rho}\frac{\partial u_i}{\partial x_i} + \frac{1}{\rho}\frac{\partial}{\partial x_i}\left(\lambda \frac{\partial T}{\partial x_i}\right) + q \tag{18}$$

where u, p, e, are velocity, static pressure and internal energy. g_i and σ_i in the momentum equation are the gravity and surface tension force. Subscripts g and l are used to represent gas and liquid phase. The advection terms of the momentum equations are estimated by the CIP (Cubic Interpolated Pseudo-particle) method [5]. The diffusion terms of the momentum equations are evaluated by the central differential scheme. The ICCG method is used to solve Poison equation of the static pressure. In the simulation code, the Cartesian coordinate system and the staggered grid are used. The surface tension in the momentum equation is estimated by use of CSF model [6]. f_m in the mass equation is volumetric fraction of gas or liquid phase. In the interface tracking method, conservation equations of f_m must be calculated:

Volumetric Fraction:

$$\frac{Df_m}{Dt} = 0 \tag{19}$$

Density:

$$\frac{D\rho_m f_m}{Dt} = -\rho_m f_m \frac{\partial u_i}{\partial x_i} \tag{20}$$

The volumetric fraction and density are calculated by the advanced interface tracking method explained in the section II.A.

3. VERIFICATION OF TPFIT CODE

We try to verify the TPFIT code with the advanced interface tracking method developed in this study by the comparison with experiments.

3.1 2-Channel Air-Water Fluid Mixing Tests

TPFIT code was applied to 2-channel air-water mixing tests. The dimension of calculated test channel is shown in Fig. 5. The test channel, which consists of two parallel subchannels with an 8 ×8 mm square cross section and the interconnection, is 220 mm long and air and water flow upwards in it. The interconnection's gap clearance,

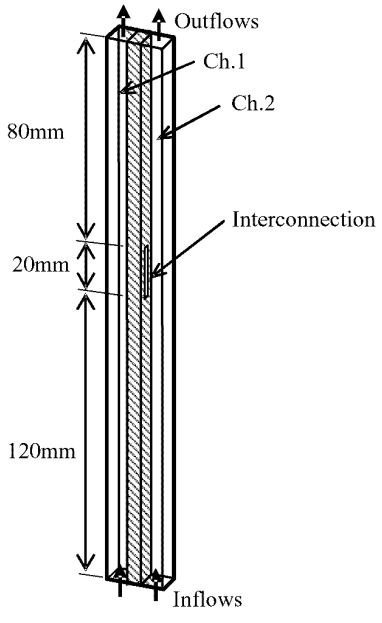

Fig. 5. Dimensions of Calculated Test Channel

horizontal and vertical lengths are 1.0 mm, 5.0 mm and 20 mm respectively. The fluid mixing was observed at interconnection in the experiments.

A non-slip wall, constant exit pressure and constant inlet velocity were selected as boundary conditions for each subchannel. The time step was controlled with a typical safety factor of 0.2 to keep it lower than the limitation value given by the Courant condition and stability condition of the CSF model [6]. In the simulation, air with 2.0cc in volume was injected into Ch. 1.

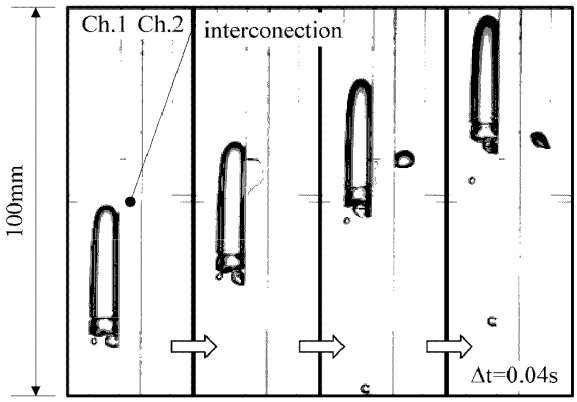

(a) Observed slug behavior

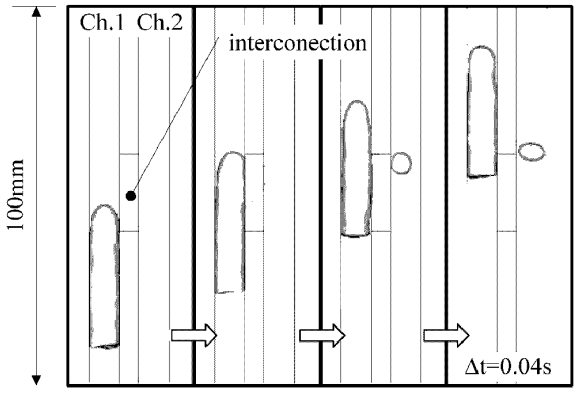

(b) Calculated results

Fig. 6. Single Bubble Behavior Around Interconnection

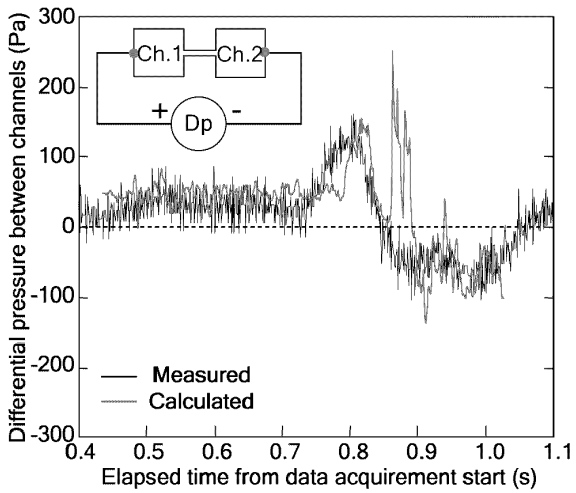

Fig. 7. Comparison Between Measured and Calculated Time Histories of Subchannel Differential Pressure

The slug behavior observed around the interconnection is shown in Fig. 6 (a). Once the top of an ascending air slug in Ch.1 reaches the center height of the interconnection, part of it starts to be drawn toward Ch. 2. Then the tip of stretched part of the air slug flows into Ch. 2 through the interconnection and is separated to form a single bubble. The calculated air slug behavior is shown in Fig. 6 (b). As shown in Fig. 6 (b), any intrusion of air into the interconnection as well as any separation of the air slug can be effectively calculated. The bubble volumes in Ch.2 are estimated to be 0.087cc in the observation and 0.094cc in the calculation. The measured and calculated time histories of the differential pressure are shown in Fig. 7. The calculated time history of the differential pressure between the channels agrees with the measured results qualitatively.

3.2 Liquid Film Falling Down on Inclined Flat Plate

The TPFIT code was applied to numerical simulation of liquid film falling down on inclined flat plate. The simulations were performed with the same conditions as the

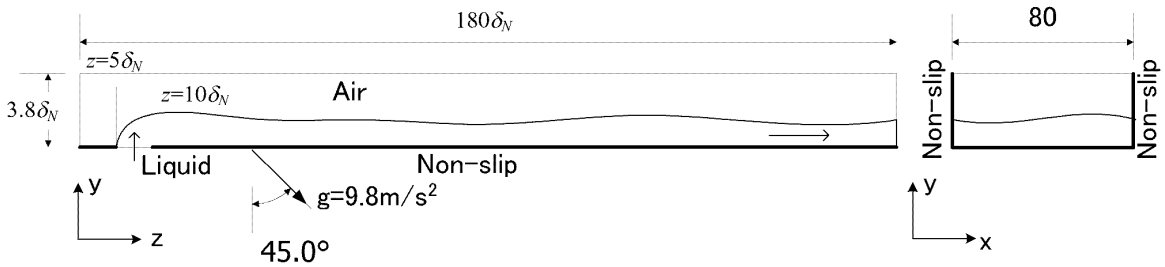

Fig. 8. Analytical Geometry of a Liquid Film.

experiment by Moran et al. [7] (see Fig. 8). Physical properties of the liquid were as follows: kinematic viscosity, ν_l=2 $\times 10^{-5}$ m^2/s, density, ρ_l=960 kg/m^3, and surface tension, σ=2.06 $\times 10^{-2}$ N/m. And air properties at 300K and atmospheric pressure were used as gas properties. On all walls, non-slip boundary condition was assigned, and inlet pressure was fixed at atmospheric pressure.

The flow conditions were summarized in Table 1. The analysis conditions were set up to compare the probability density function (PDF) of local film thickness with the experimental results. In the Table 1, δ_N represents Nusselt is mean film thickness, and is evaluated by the following equation:

$$\delta_N = \left(\frac{3\nu_l J}{g_z} \right)^{1/3} \tag{21}$$

In this equation, g_z is flow direction acceleration by gravity force, and J is volume flow rate of the liquid.

Table 1. Numerical Conditions

Case	Inlet flow rate J (l/min)	Film Reynolds number	δ_{ave_exp}	δ_{ave_cal}	δ_N
1	0.333	13	0.91	0.85	0.84
2	2.55	106	1.73	1.67	1.66
3	5.45	220	2.31	2.15	2.14

Figure 9 shows snapshot of the numerical results of the Case 3. At 0.02s, two-dimensional wave was observed near liquid inlet section, and this wave moves to the downstream section. From 0.04 seconds later, small three-dimensional waves occurred on the surface of the liquid film. After that, these small waves gradually becomes big until

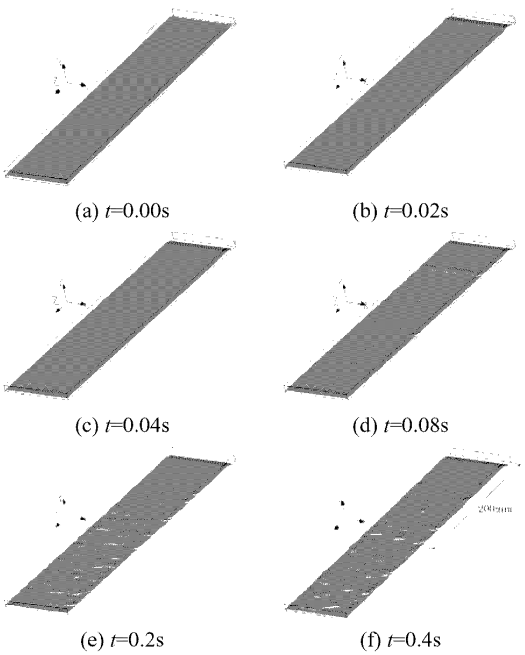

Fig. 9. Snapshot of Film Shapes

t=0.2s. At t=0.4s, the liquid film exhibited a smooth, flat gas-liquid interface upon immediate entrance to the test section, but after a short distance small, small ripples were observed at the interface. At approximately 200 mm (about z =100 δ_N) from the inlet, the small ripples developed into a three-dimensional structure characterized by large waves, and wave structures were almost developed at this point. In general, the degree of waviness increased with increasing film Reynolds number. The average local film thicknesses in the numerical result (δ_{dave_cal}) at x=20mm and z =175 δ_N are shown in Table 1 and almost agreed with Nusselt's mean film thickness. However, δ_{dave_cal} were

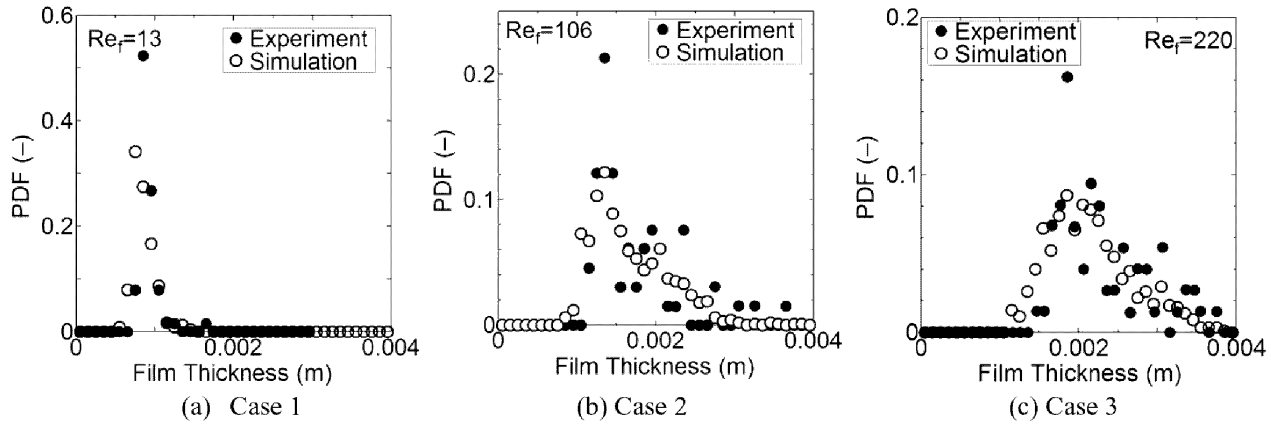

Fig. 10. Calculated PDF of Liquid Film Thickness

slightly smaller than the average film thickness in the experimental results (δ_{dave_exp}).

The probability density functions (PDF) of liquid film thickness at x=20mm and z=175 δ_N were evaluated to compare numerical results with the experimental results quantitatively. Figure 10 shows the PDF of film thickness. At low Reynolds number (Re=13), the PDF distributions showed a sharp peak (first peak) at about average film thickness, but remained close to zero for greater thickness values, indicating existence of few waves. At low film Reynolds number, the position and height of the first peak agreed well in the analysis and experiment.

In the experimental results, at relatively high Reynolds numbers (Re=106 and 220), additional smaller peak (second peak) appeared to the right of the main peak. Because the sampling number (n_s) used in the processing of the experimental data (n_s = 60) as smaller than those in the numerical result (n_s =1200), scattered results were observed in the experimental PDF distributions. As shown in Fig. 10, the numerical results agreed well with the experimental results including existence of second peaks and these positions. The predicted values of minimum liquid film thickness by the numerical simulations were slightly smaller than those measured by the experiments without relying on the mass flow rate of the liquid. It is thought that because the predicted minimum liquid film thicknesses were thin, the average liquid film thicknesses became smaller in comparison with the experimental results.

3.3 Single Bubble Behavior in Rod Bundle

The TPFIT code can treat only the Cartesian coordinate system. Therefore, complicated flow channels like the rod bundles must be modeled using a lot of rectangular numerical grids. Then, the TPFIT code was applied to single bubble behavior in the rod bundle to verify the performance of the code in complicated flow channels.

Then, we try to verify the TPFIT code by the comparison with experiments [8]. In the simulation, the flow channel is composed of a square duct and four tubes with outside diameters D=12mm as shown in Fig. 11 to simulate the experimental apparatus. In the flow channel, the tubes are used to simulate fuel rods. One center subchannel and four peripheral subchannels exist in the flow channel by these four tubes.

As the initial condition of the simulation, an air bubble was placed to the lower part of the flow channel that was filled with water. The inlet velocity of the flow channel is

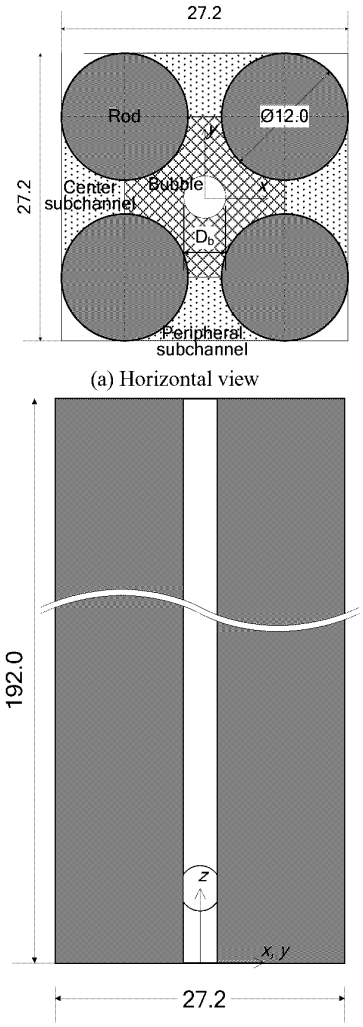

Fig. 11. Analytical Geometry

0 and the air bubble went up by the buoyancy force. The initial diameter of the bubble D_b is 4 mm, and the initial position of the air bubble is the calculation parameter of the numerical analysis. Calculation parameters used in this study are summarized in Table 2.

Figure 12 shows consecutive images of the single bubble motion. Time interval of the consecutive images is 0.02 s. The predicted terminal velocities of the bubble were about 0.24 m/s and about 20 % larger than the measured terminal velocities. The bubble exhibited either zigzag or helical motion within center subchannel. The short axes of the bubble were parallel to the traveling direction of the bubble. The wavelength of the zigzag or helical motion of the bubble was about 12.7mm, and about 10% smaller in comparison with experimental results. The terminal velocities of case that the bubble moved zigzag were larger than that it did spiral motion. These results agreed with the experimental results qualitatively.

Table 2. Calculation Parameters

	x_0 (mm)	y_0 (mm)	z_0 (mm)	D_b (mm)
Case 1	0.0	0.0	5	4
Case 1	0.8	0.8	5	4

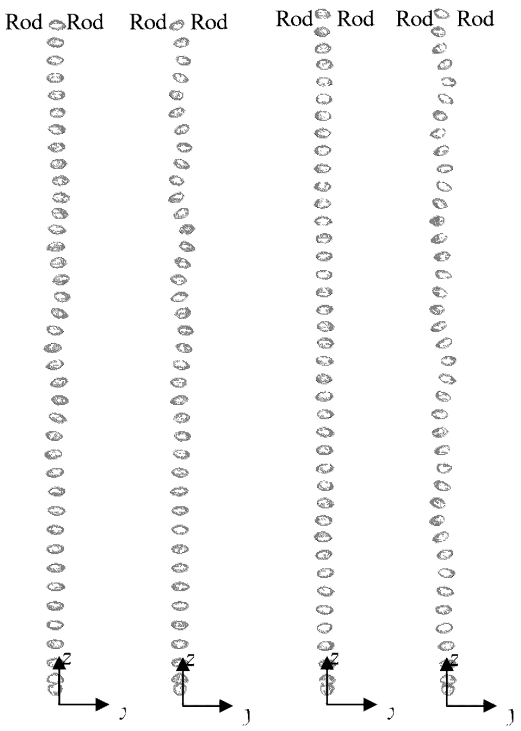

(a) Case 1 (b) Case 2

Fig. 12. Consecutive Image of Bubble Motion

4. TWO-PHASE FLOW THROUGH LIGHT-WATER REACTOR CORES

The vectorization and parallelization of TPFIT code was conducted to fit the large-scale simulations. And modified TPFIT code was applied to two-phase flow through light-water reactor cores.

4.1 Analytical Conditions

Figure 13 shows the analytical rod bundle geometry. It consists of 37 fuel rods and a hexagonal flow passage. This geometry and dimensions simulate a part of the tight-lattice fuel bundles of the RMWR core. The fuel rod outer diameter is 13 mm and the gap spacing between fuel rods is 1.3 mm. An axial length of the flow channel is 72 mm. The water flows upward from the bottom of the fuel bundle. The spacers are installed at the axial positions of 40 mm from the bottom. The axial length of the spacer is 20 mm. An example of the calculation mesh division in the horizontal cross-section is shown in Fig. 14.

Inlet conditions of water are as follows: temperature 283° C, pressure 7.2 MPa, flow rate 400 kg/m^{2}s, and the estimated Reynolds number is 40,000. On the other hand, boundary conditions are as follows: fluid velocities for x, y and z directions are zero on every wall. At the inlet of the fuel bundle, the velocity profile is uniform. The void fractions of water and vapor were varied. The computations were carried out under the non-heated isothermal flow condition.

4.2 Results and Discussion

Figure 15 shows the void fraction distributions around fuel rods in the horizontal direction. Figure 15(a) is the predicted result. Here, blue and red show water and vapor. The void fractions of blue and red indicate smaller and larger than 0.5, respectively. Each fuel rod shown with a circle is enclosed by the water film with very thin thickness, and vapor flow the outside. In the region where the gap spacing between fuel rods is narrow, the bridge formation in which adjacent fuel rods are connected by water film is confirmed. On the other hand, vapor flows through the central area of the fuel rods arranged in the shape of a triangular pitch.

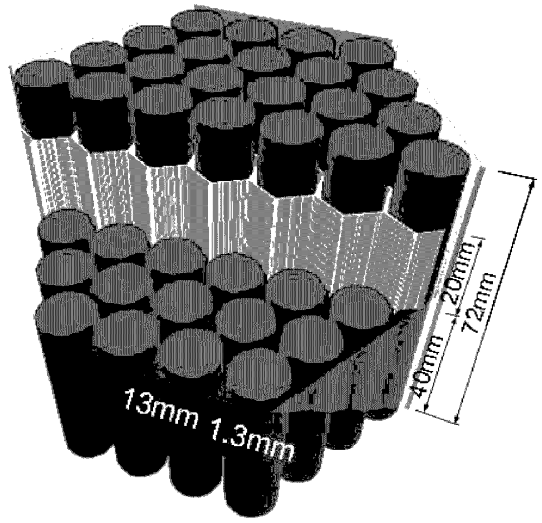

Fig. 13. A Simulated RMWR Fuel Bundle with 37 Fuel Rods and Spacer

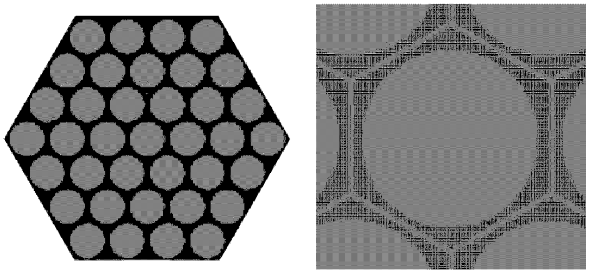

Fig. 14. An Example of Calculation Mesh Division

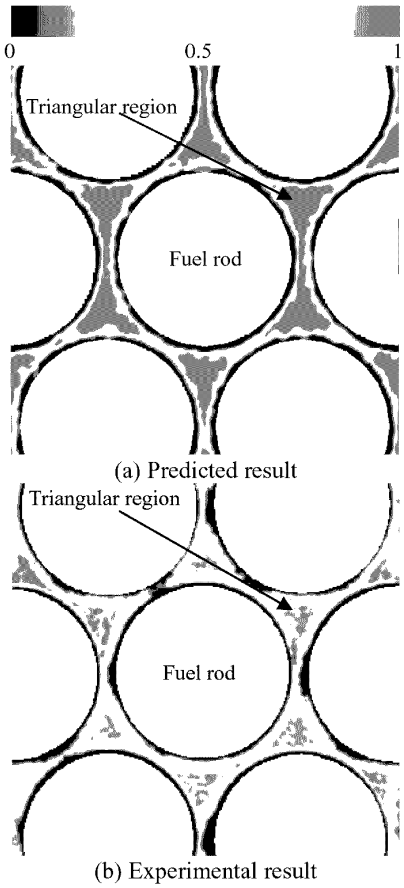

Fig. 15. Void Fraction Distributions Around Fuel Rods in the Horizontal Direction

Figure 15(b) is an example of the experimental result of the void fraction distribution obtained by an advanced neutron radiography technique [9]. Although the experiment conditions differ from the calculation conditions of Fig. 15(a) slightly, a tendency of the water and vapor distributions is in good agreement.

Water-vapor configurations under three different void fraction conditions were analyzed numerically. Figure 16 shows the predicted water-vapor configurations around a spacer. Here, Fig. 16 (a) is the case of the void fraction $\alpha = 0.9$, and Figs. (b) and (c) are the cases of $\alpha = 0.65$ and 0.4, respectively. Most of the flow area is filled with vapor when α is large. Slightly the thin water film exists on the fuel rod surface. The water-vapor configuration depends on the change of α.

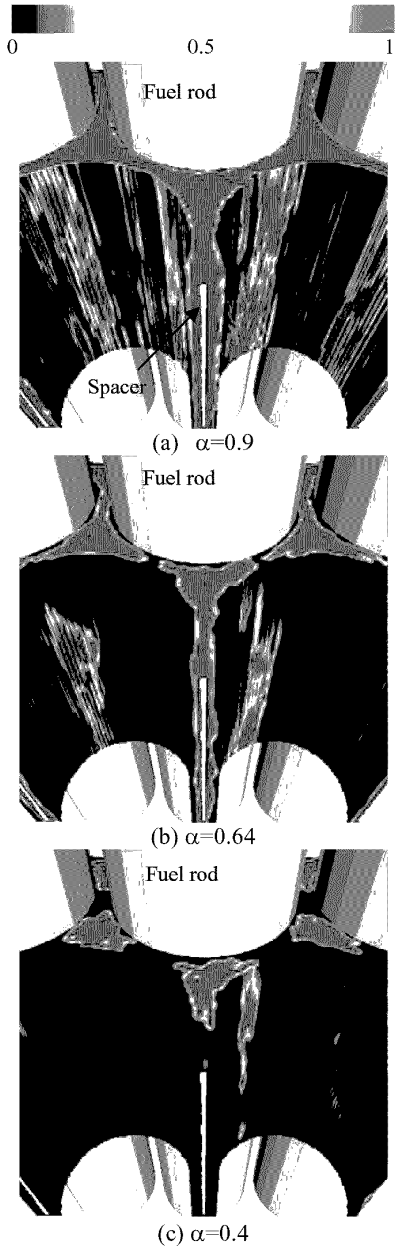

Fig. 16. APredicted Water-vapor Configurations Around a Spacer Under Three Different Void Fraction Conditions

5. CONCLUSIONS

The advanced interface tracking method to improve the conservation of volume of fluid are developed, and incorporated with two-phase flow simulation code TPFIT.

The TPFIT code was applied to experimental analyses of the 2-channel fluid mixing tests, liquid film falling down on inclined flat plate and single bubble behavior in rod bundle to examine the capability of the code. The calculated deformation and separation behavior of the air slug caused by cross flow were similar to those in observations in the 2-channel fluid mixing tests. In the results of numerical simulation of the liquid film falling down on inclined flat plate, the waves on the liquid film were observed from downstream of the inlet, and the development of the wave structures could be reproduced by the numerical simulation.

The probability density function of local film thickness agreed well with the experimental result. In the results of the single bubble behavior in rod bundle, the bubble exhibited either zigzag or helical motion within center subchannel. Also, the wavelengths of zigzag or helical motion were able to be predicted with about 10% of errors. As a result, it was confirmed that the TPFIT code can be applied to bubbly and film flow include complicated flow channels.

The TPFIT code was applied to two-phase flow through light-water reactor cores. From a series of the present predicted results it was confirmed that the large scale simulation with TPFIT was very effective for improvement of the prediction accuracy on the feasibility of the RMWR and clarification of the detailed two-phase flow configurations in the tight-lattice fuel bundle.

ACKNOWLEDGMENTS

This paper contains some results obtained within the task "Development of Fuel Assembly for Very High Burn-up Water-cooled Breeding Reactor" entrusted from the Ministry of Education, Culture, Sports, Science and Technology of Japan.

NOMENCLATURE

e : Internal energy (J/m^3)
f : Volumetric fraction (-)
g : Standard acceleration of gravity (m/s^2)
J : Mass flow rate of the liquid (kg/s)
n_m : Dimension of simulation (-)
q : Heat source (J/m^{3}s)
P : Pressure (Pa)
Re : Reynolds number (-)
u : Velocity (m/s)
t : Time (s)
x : Coordinate (m)

Greek symbols
δ : Film thickness (m)
δ_N: Average film thickness by Nusselt theory (m)
λ : Thermal conduction (J/msK)
τ : Stress tensor (m/s^2)

Subscripts
ave : Average values
cal : Calculated values
exp : Measured values
g : Gas phase
l : Liquid phase
m : gas or liquid phase

REFERENCES

[1] Dep. Nuclear Energy System, "Study on Reduced- Moderation Water Reactor (RMWR) Core Design -Joint Research Report (FY1998-1999)-", JAERI Research 2000-035, Japan Atomic Energy Research Institute (JAERI) (2000) [in Japanese].
[2] Iwamura, T., et al., "Development of reduced- moderation water reactor (RMWR) for Sustainable Energy Supply", Proc. of the 13th Pacific Basin Nuclear Conference (PBNC 2002), pp. 1631-1637, Shenzhen, China (2002).
[3] Gueyffier, D. G., et al., "Volume-of-Fluid Interface Tracking with Smoothed Surface Stress Methods for Three-Dimensional Flows", J. Comp. Physics, 152, pp.423, (1999).
[4] Yoshida, H., et al., "Numerical Simulation of Void Drift using Interface Tracking Method", Proc. of The 10th International Topical Meeting on Nuclear Reactor Thermal Hydraulics (NURETH-10), Seoul, Korea, October 5-9, E00208, (2003).
[5] Yabe, T., et al, "A universal for hyperbolic equations by cubic-polynomial interpolation", Computer Physics Communications, 66, pp.233 (1991).
[6] Brackbill, J. U., et al., "A Continuum Method for Modeling Surface Tension", J. Computational Physics, 100, pp.335 (1992).
[7] Moran, K., et al., "Instantaneous hydrodynamics of a laminar wavy liquid film", Int. J of Multiphase Flow, 28 pp.731-755 (2002).
[8] Tomiyama, A., et al., "Shapes and Rising Velocities of Single Bubbles rising through an Inner Subchannel", J. Nucl. Sci, Technol., 40 (3), pp. 136-142 (2003).
[9] Kureta, M., et al., "Measurement of Vapor Behavior in Tight -Lattice Bundles by Neutron Radiography", Proc. of the 6th International Conference on Nuclear Thermal Hydraulics, Operations and Safety (NUTHOS-6), Nara, Japan, October 4-8, N6P200 (2004).